Passive Near-Field Mixing Enhancement in Rectangular Jet Flows

W. R. Quinn*
St. Francis Xavier University, Antigonish, Nova Scotia, B2G 1C0 Canada

This paper presents the results of an experimental study of the near flowfields of turbulent free air jets issuing from sharp-edged rectangular slots of aspect ratio 2 and 10. The results, which include the mean streamwise velocity, the turbulence kinetic energy, the Reynolds shear stress and the transport of some of the Reynolds stresses, were obtained with hot-wire anemometry. Saddle-shaped mean streamwise velocity profiles, which were absent in the flow issuing from the slot of aspect ratio 2, were found in the flow issuing from the slot of aspect ratio 10 in the central plane of the slot major axis. In the very near flowfield (i. e., $X/D_e \leq 5$), higher shear-layer values of the turbulence kinetic energy and the Reynolds shear stress, indicating enhanced near-field mixing, were found where the saddle-shaped mean streamwise velocity profiles existed.

Nomenclature

A,B	= constants in hot-wire exponent power law
D_e	= equivalent diameter of slot
E	= hot-wire output voltage
n	= exponent in hot-wire exponent power law
q^2	= turbulence kinetic energy $[(\overline{u'^2} + \overline{v'^2} + \overline{w'^2})/2]$
U	= mean streamwise velocity
$\overline{u'v'}$	= Reynolds shear stress in the X-Y plane
$\overline{u'^2v'}$	= transport of the Reynolds normal stress $\overline{u'^2}$
$\overline{u'v'^2}$	= transport of the Reynolds shear stress $\overline{u'v'}$
$\overline{u'w'}$	= Reynolds shear stress in the X-Z plane
$\overline{v'^3}$	= transport of the Reynolds normal stress $\overline{v'^2}$
$\overline{w'^2}$	= Reynolds normal stress
X	= streamwise coordinate
Y	= spanwise coordinate
$Yhlf$	= jet velocity half-width in the Y direction
Z	= lateral coordinate
$Zhlf$	= jet velocity half-width in the Z direction

Subscripts

Cl	= centerline value
max	= maximum value

Introduction

RECTANGULAR turbulent free jets find use in technical applications in aerospace and mechanical engineering. In V/STOL aircraft, for example, rectangular jets issuing normal to the wing are used for powered lift. Rectangular jets have, therefore, been studied by a number of investigators.[1-14] The practical demands of speed of manufacturing and ease of installation make it necessary to use sharp-edged slots in some applications. Turbulent free jets issuing from such sharp-edged rectangular slots have also received some attention.[3,4,6-8,10-12] It has been found that the near-field mean streamwise velocity distribution, in the plane containing the major axis of the slot, has a saddle (or U) shape. The saddle shape is more pronounced in jets issuing from sharp-edged slots,[3,4,6] as opposed to those issuing from short converging nozzles.[1,2] This saddle-shaped mean streamwise velocity distribution results, as will be shown, in near-field mixing enhancement that, for weight reasons, is important in aircraft applications. No previous study has examined the effect of the presence or absence of saddle-shaped mean streamwise velocity profiles on near-field mixing in rectangular jet flows.

The present experimental study, therefore, investigates this aforementioned aspect of turbulent free jets issuing from sharp-edged rectangular slots. Two slot aspect ratios (2 and 10), with the same exit-plane area, are used. The exit-plane Reynolds number, based on the equivalent diameter of the slot (same as the diameter of a round slot with the same exit area as the rectangular slot), was about 2.08×10^5 in both flows considered. The mean streamwise velocity and streamwise turbulence intensity at the center of the slot exit plane were kept at 60 m/s and 0.5%, respectively, in the two jets.

Experimental Rig and Procedure

The blow-down jet flow facility used in the present study has been described in detail elsewhere.[15] Briefly, the jet flow facility consists of a centrifugal fan, a settling chamber fitted with honeycomb and mesh-wire screens, a three-dimensional contraction with a contour based on a third-degree polynomial, and the sharp-edged rectangular slots. The slots are used to cap the downstream end of the three-dimensional contraction. Each slot is assembled from four machine-mitred pieces of aluminum, two of which are shown, for the slot of aspect ratio 10, in Fig. 1 along with the coordinate system. The jets issue into a cage that is covered on the top and sides with

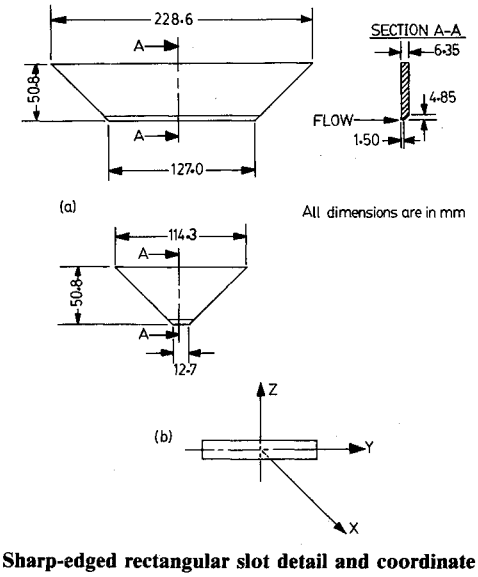

Fig. 1 Sharp-edged rectangular slot detail and coordinate system.

Received Oct. 6, 1989; revision received March 9, 1990.

*Associate Professor. Member AIAA

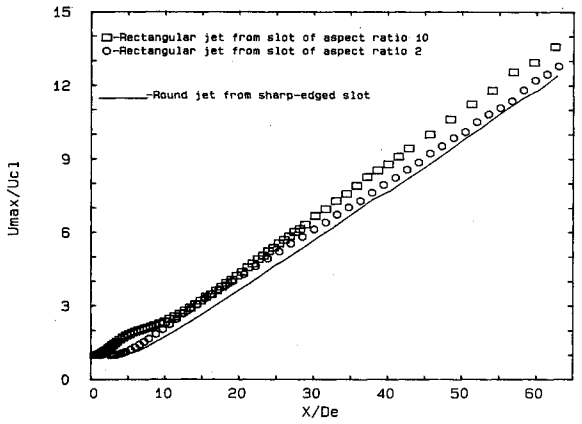

Fig. 2 Mean streamwise velocity decay plots.

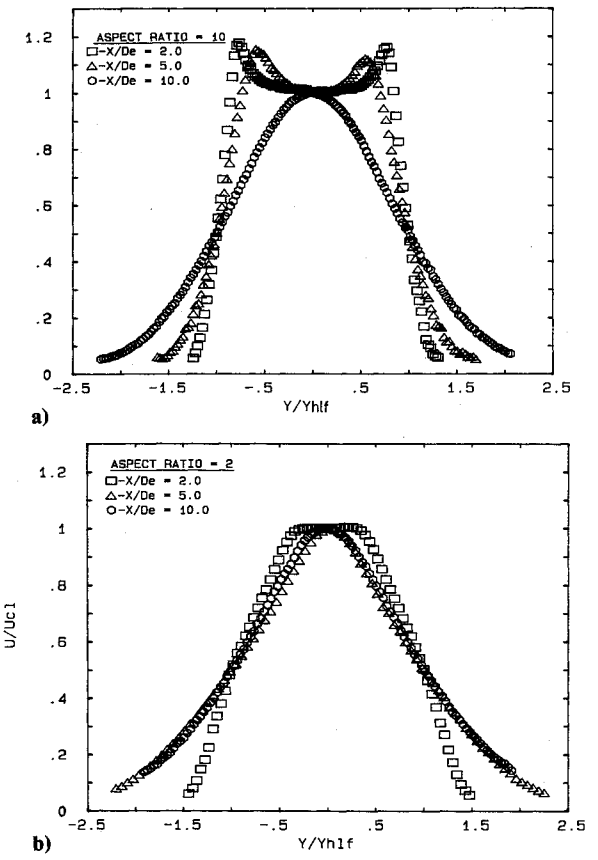

Fig. 3 Mean streamwise velocity profiles in the central X-Y plane.

steel damping screens of 42% porosity. The screens help to minimize the effect of room drafts. The upstream end of the cage, which extends 3.66 m downstream, is fitted with a 2.44 × 2.44 m plywood wall that is flush with the downstream end of the three-dimensional contraction. The downstream end of the cage is open.

A three-dimensional traversing system, driven by stepping motors under microcomputer control, was used for traversing the sensing probe in the flowfield. The traversing system consists of a rack and pinion for probe movement in the streamwise direction and lead screws for moving the probe in the spanwise and lateral directions. The sensing probe could be positioned to within 0.3 mm in the streamwise direction and to within 0.01 mm in the spanwise and lateral directions.

The mean and fluctuating velocities were acquired with X-array hot-wire probes manufactured by DANTEC. The hot-wire probes, operated by constant temperature anemometers at a resistance ratio of 1.8, were calibrated on-line on the jet

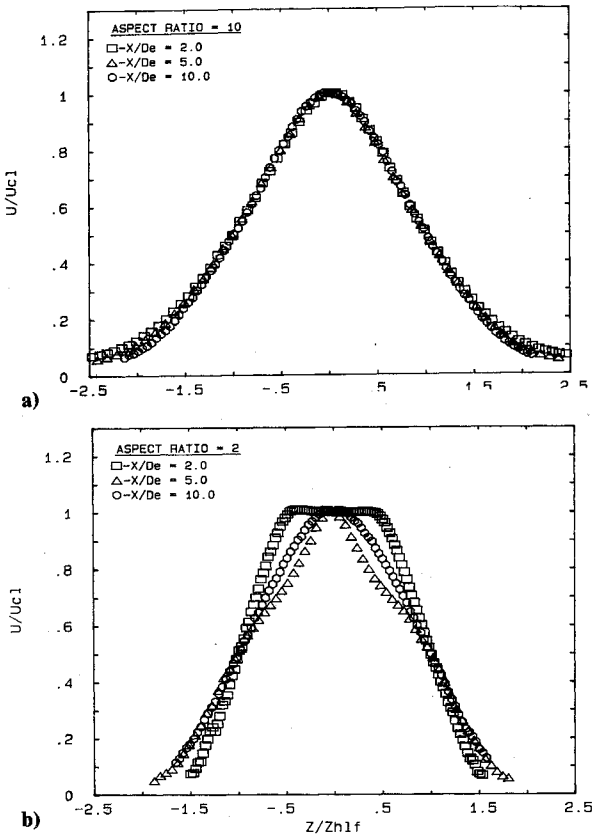

Fig. 4 Mean streamwise velocity profiles in the central X-Z plane.

centerline in the very near flowfield against the output of a pitot-static tube that was connected to a pressure transducer and a Barocel electronic manometer. The calibration data were fitted to the exponent power law: $E^2 = A + BU^n$ and A, B, and n were optimized using a linear least-squares goodness-of-fit procedure. A "cosine law" response to yaw was assumed and the effective angle was determined from a yaw calibration as described by Bradshaw.[16] The hot-wire signals were linearized by a microcomputer and digitized, at about 1 kHz, by a 12-bit A/D converter of the successive approximation type. A two-channel sample-and-hold unit with very low droop rate, two low-pass analog filters, and amplifiers were used for signal processing and signal conditioning. The data reduction was performed in real time using the laboratory microcomputer. Temperature variations from the calibration temperature were monitored with a thermocouple placed close to the hot-wire probe and corrections for such variations were made, following the procedure in Bearman,[17] in the data-reduction software. The correction formulae, for the effect of tangential cooling of X-array hot-wire probes proposed by Champagne and Steicher,[18] were also incorporated in the data-reduction software.

Results and Discussion

The estimated uncertainties in the quantities measured directly are as follows: U: ±1%, $\overline{u'^2}$, $\overline{v'^2}$, and $\overline{w'^2}$: ±6%, $\overline{u'v'}$ and $\overline{u'w'}$: ±8%, all of which are at 20:1 odds.

The decay of the mean streamwise velocity along the jet centerline is shown in Fig. 2 for the two rectangular jets (which will, in what follows, be referred to as the aspect ratio 10 jet and the aspect ratio 2 jet) and, for comparison, for the round jet issuing from a sharp-edged slot. While the aspect ratio 2 jet decays linearly after the potential core and a short transition region, linear decay for the aspect ratio 10 jet is preceded by a nonlinear or power-law decay region that follows the potential core. Sforza and his co-workers[1,2,5] have named this nonlinear decay region the characteristic decay region because it is influenced directly by the shape and aspect ratio of a slot or noz-

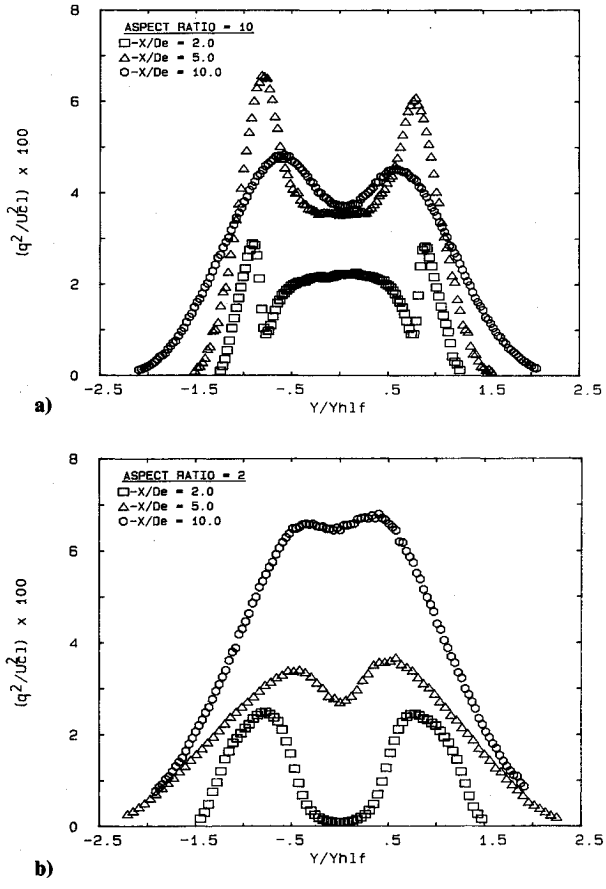

Fig. 5 Turbulence kinetic energy profiles in the central X-Y plane.

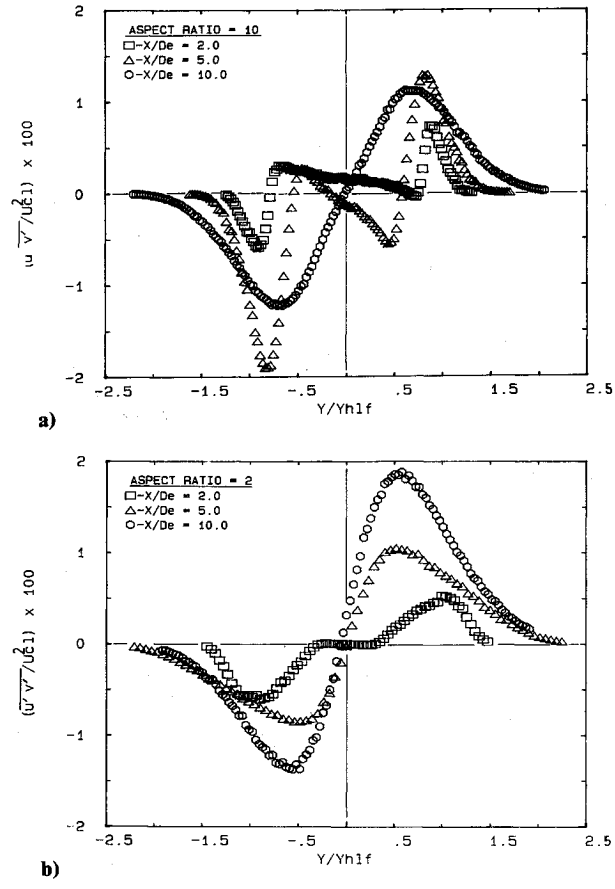

Fig. 7 Reynolds shear-stress profiles in the central X-Y plane.

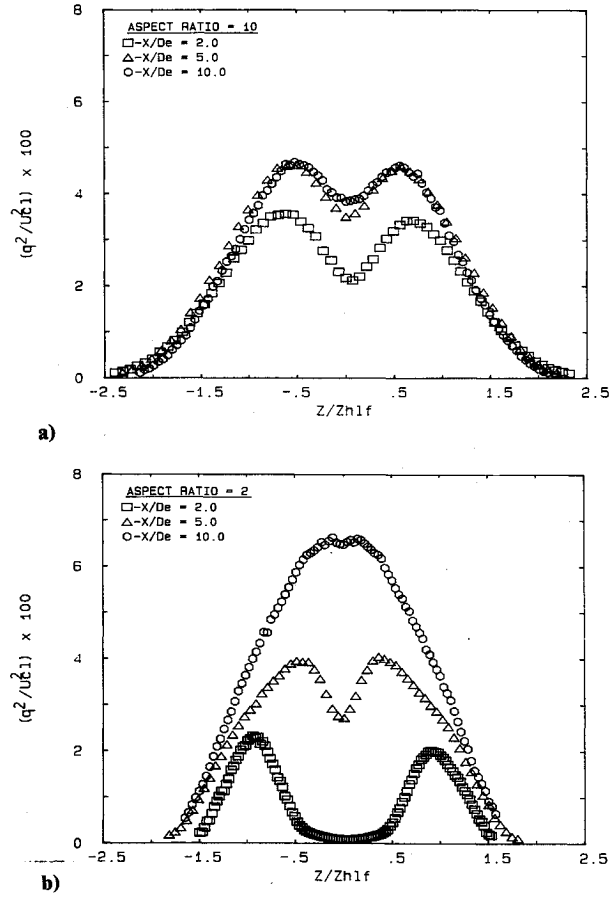

Fig. 6 Turbulence kinetic energy profiles in the central X-Z plane.

zle. The potential core lengths, deduced from Fig. 2, are $0.86D_e$, $2.51D_e$, and $4.4D_e$ for the aspect ratio 10 jet, the aspect ratio 2 jet, and the round jet, respectively. The most rapid near-field mixing should occur in the aspect ratio 10 jet because it has the shortest potential core length.

The near-field mean streamwise velocity profiles in the central plane of the slot major axis (X-Y) are presented in Fig. 3 and those in the central plane of the slot minor axis (X-Z) are presented in Fig. 4. Saddle-shaped mean streamwise velocity profiles, which have also been observed in rectangular jet flows by others[1-12] and by Gutmark and Schadow[19] in a tapered elliptic jet, are clearly evident in the X-Y plane within the characteristic decay region of the aspect ratio 10 jet (Fig. 3a). It should be noted that the saddle-shaped mean streamwise velocity profiles are characterized by steep gradients. By contrast, such saddle-shaped mean streamwise velocity profiles are absent in the aspect ratio 2 jet in both planes of symmetry (Figs. 3b and 4b) and in the X-Z plane of the aspect ratio 10 jet (Fig. 4a). The self-similar mean streamwise velocity profiles found in the X-Z plane of the aspect ratio 10 jet (Fig. 4a) provide further evidence of the faster development of the jet compared to that of the aspect ratio 2 jet in which a core still exists at $X/D_e = 2$ in the X-Z plane (Fig. 4b).

Turbulence kinetic energy profiles are presented in Figs. 5 and 6. Note that all three normal stresses, $\overline{u'^2}$, $\overline{v'^2}$, and $\overline{w'^2}$, were measured. Moreover, the measurements were made only in the central X-Y and X-Z planes. In the very near flowfield (i.e., $X/D_e = 2$ and 5), the shear-layer values of the turbulence kinetic energy, in both planes of symmetry, are generally higher in the aspect ratio 10 jet (Figs. 5a and 6a) than in the aspect ratio 2 jet (Figs. 5b and 6b). This behavior is consistent with the expected, more rapid near-field mixing of the aspect ratio 10 jet, because of its shorter potential core length, as mentioned earlier. The highest turbulence kinetic energy values, in this near-field region of the flow, are found at X/D_e

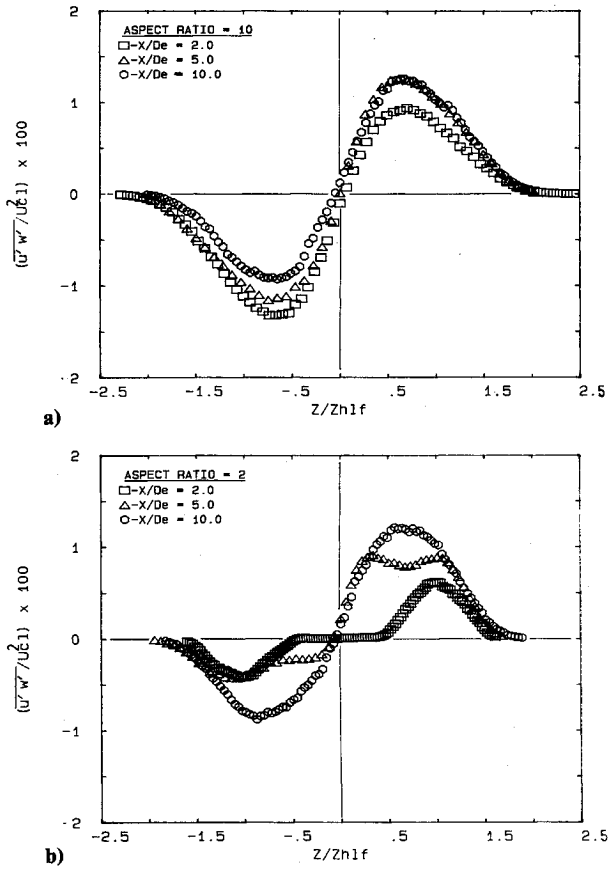

Fig. 8 Reynolds shear-stress profiles in the central X-Z plane.

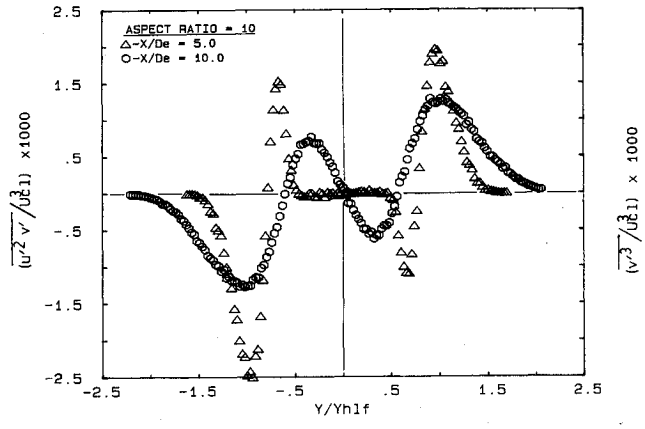

Fig. 9a Transport of the Reynolds normal stress $\overline{u'^2}$ in the central X-Y plane.

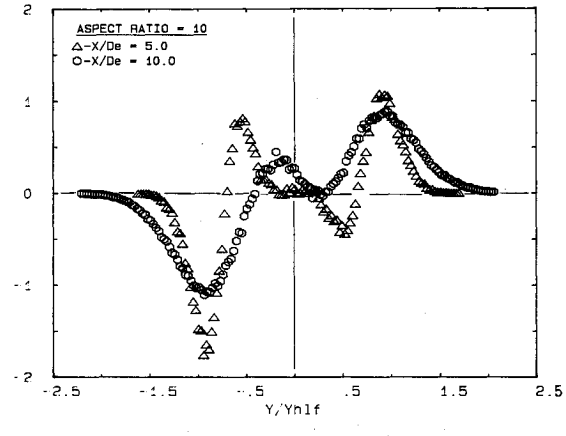

Fig. 9b Transport of the Reynolds normal stress $\overline{v'^2}$ in the central X-Y plane.

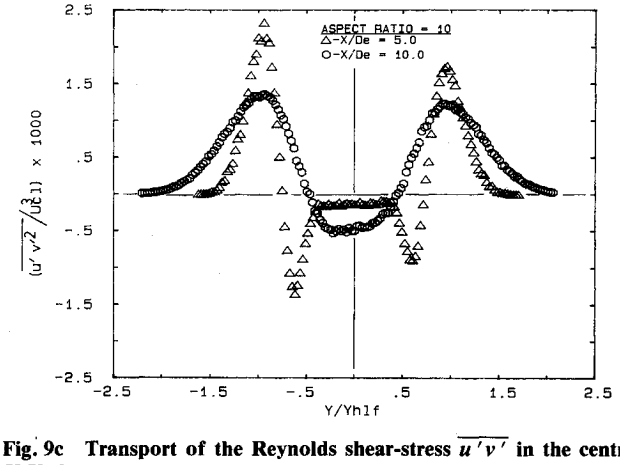

Fig. 9c Transport of the Reynolds shear-stress $\overline{u'v'}$ in the central X-Y plane.

$= 5$ in the X-Y plane of the aspect ratio 10 jet. It should be recalled that saddle-shaped mean streamwise velocity profiles occur at this location (Fig. 3a). The marked decrease in the turbulence kinetic energy within the shear layer at $X/D_e = 10$ compared to that at $X/D_e = 5$ in the X-Y plane of the aspect ratio 10 jet (Fig. 5a) is due to the merging of the shear layers emanating from the shorter sides of the slot and the concomitant decrease in turbulent activity. In general, high values of the turbulence kinetic energy are found where the local shear in the mean streamwise velocity is high and vice versa. For example, for the aspect ratio 10 jet at $X/D_e = 5$ in the central X-Y plane, the peak values of the turbulence kinetic energy are at $Y/Yhlf = 0.787$ and at $Y/Yhlf = -0.821$, which are the locations where $\partial(U/U_{Cl})/\partial(Y/Yhlf)$ takes on extreme (i.e., maximum or minimum) values. This close correlation between q^2 and the mean streamwise velocity gradient suggests that production due to $\partial(U/U_{Cl})/\partial(Y/Yhlf)$ and $\partial(U/U_{Cl})/\partial(Z/Zhlf)$ dominates the production of q^2 in the central X-Y and X-Z planes, respectively.

As in all turbulent free jets issuing into a still ambient, high local turbulence intensities also occur on the low-velocity sides of the jets of the present investigation. The fact that the yaw response of the X-array hot-wire probe was not extended in the present study will not, according to the findings of Browne et al.,[20] have any bearing on the $\overline{u'^2}$, $\overline{u'v'}$, and $\overline{u'w'}$ results, but will cause a slight overestimation of the $\overline{v'^2}$ and $\overline{w'^2}$ results and thus the q^2 results.

Reynolds shear-stress profiles are presented in Figs. 7 and 8. Like the turbulence kinetic energy, the shear-layer values of the Reynolds shear stress, in both planes of symmetry, are higher in the aspect ratio 10 jet in the very near flowfield (Figs. 7a and 8a). This further attests to the expected, more rapid mixing of the aspect ratio 10 jet. As is the case with the turbulence kinetic energy, production due to the mean streamwise velocity gradients appears to be the dominant contribution to Reynolds shear-stress production since the mean streamwise velocity gradient distribution correlates well with the Reynolds shear-stress distribution.

The transport of the Reynolds stresses $\overline{u'^2}$, $\overline{v'^2}$, and $\overline{u'v'}$, for the aspect ratio 10 jet in the central X-Y plane, is presented in Fig. 9. Such data will aid the modeling of the turbulent transport terms in Reynolds-stress modeling. The high shear-layer values of the turbulence kinetic energy and Reynolds shear stress at $X/D_e = 5$ are reflected in the turbulent transport of the Reynolds stresses shown in Fig. 9.

Conclusions

The present experimental study of the near flowfields of turbulent free air jets issuing from sharp-edged rectangular slots

of aspect ratio 2 and 10 has documented a new set of mean flow and turbulence data. The data include the mean streamwise velocity, the turbulence kinetic energy, the Reynolds shear stress, and the transport of some of the Reynolds stresses.

Saddle-shaped mean streamwise velocity profiles, which were absent in the flow issuing from the slot of aspect ratio 2, were found in the flow issuing from the slot of aspect ratio 10 in the central plane of the slot major axis. In the very near flowfield (i.e., $X/D_e \leq 5$), higher shear-layer values of the turbulence kinetic energy and the Reynolds shear stress, consistent with the expected more rapid mixing of the aspect ratio 10 jet because of its shorter potential core length, were found where the saddle-shaped mean streamwise velocity profiles existed.

Acknowledgment

The support of the Natural Sciences and Engineering Research Council of Canada, through Grant A5484, is gratefully acknowledged.

References

[1]Sforza, P. M., Steiger, M. H., and Trentacoste, N., "Studies on Three-Dimensional Viscous Jets," *AIAA Journal*, Vol. 4, No. 5, 1966, pp. 800–806

[2]Trentacoste, N., and Sforza, P. M., "Further Experimental Results for Three-Dimensional Free Jets," *AIAA Journal*, Vol. 5, No. 5, 1967, pp. 885–891.

[3]Sfeir, A. A., "The Velocity and Temperature Fields of Rectangular Jets," *International Journal of Heat and Mass Transfer*, Vol. 19, Aug. 1976, pp. 1289–1297.

[4]Sfeir, A. A., "Investigation of Three-Dimensional Turbulent Rectangular Jets," *AIAA Journal*, Vol. 17, No. 10, 1979, pp. 1055–1060.

[5]Sforza, P. M., and Stasi, W., "Heated Three-Dimensional Turbulent Jets," *Journal of Heat Transfer*, Vol. 101, May 1979, pp. 353–358.

[6]Marsters, G. F., "The Effects of Upstream Nozzle Shaping on Incompressible Turbulent Flows from Rectangular Nozzles," *Transactions of CSME*, Vol. 5, No. 4, 1978–79, pp. 197–203.

[7]Marsters, G. F., and Fotheringham, J., "The Influence of Aspect Ratio on Incompressible, Turbulent Flows from Rectangular Slots," *The Aeronautical Quarterly*, Vol. 31, Pt. 4, Nov. 1980, pp. 285–305.

[8]Marsters, G. F., "Spanwise Velocity Distributions in Jets from Rectangular Slots," *AIAA Journal*, Vol. 19, No. 2, 1981, pp. 148–152.

[9]Krothapalli, A., Baganoff, D., and Karamcheti, K., "On the Mixing of a Rectangular Jet," *Journal of Fluid Mechanics*, Vol. 107, June 1981, pp. 201–220.

[10]Quinn, W. R., Pollard, A., and Marsters, G. F., "Measurements in a Turbulent Rectangular Free Jet," *Proceedings of the 4th Symposium on Turbulent Shear Flows*, Univ. of Karlsruhe, Karlsruhe, Germany, Sept. 1983, pp. 7.1–7.6.

[11]Quinn, W. R., Pollard, A., and Marsters, G. F., "Mean Velocity and Static Pressure Distributions in a Three-Dimensional Turbulent Free Jet," *AIAA Journal*, Vol. 23, No. 6, 1985, pp. 971–973.

[12]Tsuchiya, Y., Horikoshi, C., and Sato, T., "On the Spread of Rectangular Jets," *Experiments in Fluids*, Vol. 4, No. 4, 1986, pp. 197–204.

[13]Gutmark, E., Schadow, K. C., and Wilson, K. J., "Noncircular Jet Dynamics in Supersonic Combustion," *Journal of Propulsion and Power*, Vol. 5, No. 5, 1988, pp. 529–533.

[14]Morrison, G. L., and Swan, D. H., "Three-Dimensional Flow Field Measurements of a 4:1 Aspect Ratio Subsonic Jet," AIAA Paper 89-1092, April 1989.

[15]Quinn, W. R., and Militzer, J., "Experimental and Numerical Study of a Turbulent Free Square Jet," *Physics of Fluids*, Vol. 31, No. 5, 1988, pp. 1017–1025.

[16]Bradshaw, P., *An Introduction to Turbulence and Its Measurement*, Pergamon, Oxford, England, UK, 1975.

[17]Bearman, P. W., "Corrections for the Effect of Ambient Temperature Drift on Hot-Wire Measurements in Incompressible Flow," *DISA Information*, Vol. 11, May 1971, pp. 25–30.

[18]Champagne, F. H., and Sleicher, C. A., "Turbulence Measurements with Inclined Hot-Wire Probes—Part 2: Hot-Wire Response Equations," *Journal of Fluid Mechanics*, Vol. 28, Part 1, 1967, pp. 177–182.

[19]Gutmark, E., and Schadow, K. C., "Flow Characteristics of Orifice and Tapered Jets," *Physics of Fluids*, Vol. 30, Nov. 1987, pp. 3448–3454.

[20]Browne, L. W. B., Antonia, R. A., and Chua, L. P., "Calibration of X-Probes for Turbulent Flow Measurements," *Experiments in Fluids*, Vol. 7, No. 3, 1989, pp. 201–208.